# Gapless fracton quantum spin liquid and emergent photons in a 2D spin-1 model

Nils Niggemann,[1, 2, 3, *] Meghadeepa Adhikary,[4, 5] Yannik Schaden-Thillmann,[2, 3] and Johannes Reuther[2, 3]

[1] *The Abdus Salam International Center for Theoretical Physics (ICTP), Strada Costiera 11, I-34151 Trieste, Italy*
[2] *Helmholtz-Zentrum Berlin für Materialien und Energie, Hahn-Meitner Platz 1, 14109 Berlin, Germany*
[3] *Dahlem Center for Complex Quantum Systems and Fachbereich Physik,*
*Freie Universität Berlin, 14195 Berlin, Germany*
[4] *Department of Physics and Quantum Centers in Diamond and Emerging Materials (QuCenDiEM) group,*
*Indian Institute of Technology Madras, Chennai 600036, India*
[5] *SISSA, Via Bonomea 265, I-34136 Trieste, Italy*
(Dated: August 29, 2025)

## I. NUMBER OF CLASSICAL GROUND STATES

We derive an estimate for the dimension $n$ of the constrained Hilbert space in which $\mathcal{C}_{\boxtimes} = 0$ for all eight-site clusters centered around $\boxtimes$. Particularly, for a system with $N_{\text{sites}}$ spins we express $n$ as $n = b^{N_{\text{sites}}}$ and calculate the base $b$.

A simple estimate, following from Pauling counting arguments approximates $n$ as $n \approx 3^{N_{\text{sites}}} k^{N_{\text{sites}}/2}$ with the total number of spin-1 Ising configurations given as $3^{N_{\text{sites}}}$ and defining $k$ as the ratio between the number of all configurations satisfying $\mathcal{C}_{\boxtimes} = 0$ for one cluster $\boxtimes$ and the total number of $3^8$ Ising configurations in one cluster. Furthermore, $N_{\text{sites}}/2$ is the number of constraints. This approximation gives $b \approx \sqrt{41/27} = 1.232$.

More rigorously, we may also determine $b$ by systematically calculating upper and lower bounds. For estimating an upper bound of $b$, we consider systems with periodic boundaries and $N_{\text{sites}} = L \times L$ sites. Specifically, we determine $n$ for $L = 4$ and $L = 6$ by exhaustively generating all states in the constrained subspace. We note that for $L > 6$ this becomes numerically too difficult due to the large number of states. The obtained values are given in Table I together with the base $b$ calculated through $b = n^{1/L^2}$. The base $b$ for $L = 6$ is smaller than for $L = 4$ and therefore the value $b = 1.541$ for $L = 6$ can be used as an upper bound.

A lower bound of $b$ is found by determining the exact number of states that are obtained by applying fluctuator moves in the configuration of Fig. 1(a). This state has a $\sqrt{10} \times \sqrt{10}$ unit cell indicated by red dashed lines and it has one flippable cluster per unit cell (their centers are marked by red dots). Importantly, these flippable clusters do not overlap such that they can be flipped independently. Furthermore, under the condition that flippable clusters do not overlap, their density (one flippable cluster per 10 sites) is maximal in this state. Since each flippable cluster can be in three different configurations, fluctuator moves starting from Fig. 1(a) can generate $3^{N_{\text{sites}}/10}$ different states in the constrained subspace,

| | Number of states $n$ | $b = n^{1/L^2}$ |
|---|---|---|
| $L = 4$ | 6859 | 1.737 |
| $L = 6$ | 5800827 | 1.541 |

TABLE I. Dimension $n$ of the constrained subspace for a system with periodic boundaries and $N_{\text{sites}} = L \times L$ sites, where $L = 4$ and $L = 6$. The third column shows the base $b$ defined by $n = b^{N_{\text{sites}}}$.

yielding the lower bound $b = 3^{1/10} = 1.116$. In total, one finds

$$b = 1.329 \pm 0.213, \qquad (1)$$

where the error margins range up (down) to the upper (lower) bounds, which agrees with the Pauling estimate. We note that in the case of spin-1/2, the Pauling estimate is found to be surprisingly inaccurate, see Ref. [1] for details.

## II. HILBERT SPACE FRAGMENTATION

The dynamics generated by the fluctuators $\mathcal{F}_{\square}$ and $\mathcal{F}_{\square}^{\dagger}$ does not cover the full constrained subspace of the spin-1 spiderweb model, but splits it into many dynamically disconnected sectors. This property, referred to as Hilbert space fragmentation is known from other fracton models [2–8]. Here, we prove the existence of Hilbert space fragmentation for the spiderweb model, i.e. that the number of dynamically disconnected sectors grows exponentially with the number of sites. While we focus on the case of spin 1, we note that this argument holds for any spin, in particular also spin-1/2, see Ref. [1].

For our proof we consider a new type of fluctuator $\mathcal{F}_{\boxplus}$ shown in Fig. 1(b). Its action on a 14-site cluster flips 12 of these spins by two units of angular momentum (i.e. locally acts as $S_i^+ S_i^+$ or $S_i^- S_i^-$) but does not change the two center spins [marked with numbers 1 and 2 in Fig. 1(b)]. Importantly, $\mathcal{F}_{\boxplus}$ is defined in a way that it annihilates states where the center spins 1 and 2 are not equal or when they are both in $S^z = 0$ configurations. This may be enforced, via the simple projector $\left[1 - \frac{1}{4} \left(S_1^z - S_2^z\right)^2\right] \times \left(S_1^z\right)^2 \left(S_2^z\right)^2$. In the illustrated case,

---

the center spins have $S^z = 1$, however, our arguments also apply to the case where they are in $S^z = -1$ configurations.

If one only considers the net changes $\Delta S_i^z$ at these 14 sites, the fluctuator $\mathcal{F}_{\boxplus}$ is identical to $\mathcal{F}_{\square}\mathcal{F}_{\square}\mathcal{F}_{\square'}\mathcal{F}_{\square'}$ acting on two eight-site clusters centered around the sites $\square$ and $\square'$ ($\square$ and $\square'$ are those sites that both have the sites 1 and 2 as their nearest neighbors). Therefore, $\mathcal{F}_{\boxplus}$ and $\mathcal{C}_{\boxtimes}$ commute for all $\boxtimes$ which means that $\mathcal{F}_{\boxplus}$ operates *within* the constrained subspace. However, if one now considers the consecutive execution of the four operators $\mathcal{F}_{\square}$, $\mathcal{F}_{\square}$, $\mathcal{F}_{\square'}$, $\mathcal{F}_{\square'}$ one finds that there is no order in which these operators can be applied such that they act like $\mathcal{F}_{\boxplus}$, since they always annihilate the state in Fig. 1(b). This is due to the condition that the two center spins 1 and 2 fulfill $S_1^z \neq 0$, $S_2^z \neq 0$ and $S_1^z = S_2^z$. In other words, the action of the double fluctuator $\mathcal{F}_{\boxplus}$ on these 14 sites cannot be expressed as the sequential action of $\mathcal{F}_{\square}$ and $\mathcal{F}_{\square'}$. Consequently, the two 14-site states in Fig. 1(b) are in different Hilbert space sectors under the action of $\mathcal{F}_{\square}$ (and $\mathcal{F}_{\square}^{\dagger}$).

The property that $\mathcal{F}_{\boxplus}$ creates new Hilbert space sectors is often no longer given if the motif in Fig. 1(b) is part of a larger system with more than 14 sites. This is because in a larger system it may be possible to express $\mathcal{F}_{\boxplus}$ as

$$\mathcal{F}_{\boxplus} = \cdots \mathcal{F}_{\square} \cdots \mathcal{F}_{\square} \cdots \mathcal{F}_{\square'} \cdots \mathcal{F}_{\square'} \cdots , \qquad (2)$$

where "$\cdots$" denotes fluctuator moves $\mathcal{F}$ on other surrounding eight-site clusters. To prove the exponential scaling of the number of Hilbert-space sectors it is, however, sufficient to find *one* periodic state with the motif in Fig. 1(b) and where $\mathcal{F}_{\boxplus}$ cannot be expressed via elementary fluctuators $\mathcal{F}_{\square}$ as in Eq. (2). Such a configuration is shown in Fig. 1(c) which has a $4 \times 4$ unit cell containing the motif in Fig. 1(b). Another configuration with this property is discussed in Ref. [1]. Note that the action of the double fluctuator $\mathcal{F}_{\boxplus}^{\dagger}$ is illustrated in the center $4 \times 4$ unit cell of Fig. 1(c). Importantly, none of the states obtained by applying $\mathcal{F}_{\boxplus}^{(\dagger)}$ in different unit cells has eight-site clusters that can be flipped by $\mathcal{F}_{\square}$ or $\mathcal{F}_{\square}^{\dagger}$. Consequently, the action of $\mathcal{F}_{\boxplus}^{\dagger}$ in any $4 \times 4$ unit cell leads to a new Hilbert space sector. A lower bound for the number of sectors can now be estimated as $2^{N_{\text{sites}}/16}$, demonstrating its exponential scaling with system size. However, note that each of these sectors is trivial in the sense that it contains only a single state.

We emphasize that in a generic spin-1 configuration with the 14-site motif in Fig. 1(b) the action of $\mathcal{F}_{\boxplus}$ will usually *not* result in a new sector because $\mathcal{F}_{\boxplus}$ can be expressed as in Eq. (2). In the rare exceptions [Fig. 1(c)] the creation of new Hilbert space sectors via $\mathcal{F}_{\boxplus}$ is only possible because the 14-site motif is trapped in an environment with inactive or severely limited $\mathcal{F}_{\square}$-dynamics (e.g. due to the absence of local $S_i^z = 0$ states). Stated differently, we could not find a spin-1 state where the application of $\mathcal{F}_{\boxplus}$ creates a new sector while the $\mathcal{F}_{\square}$-dynamics in these sectors is connected and can spread over the whole sys-
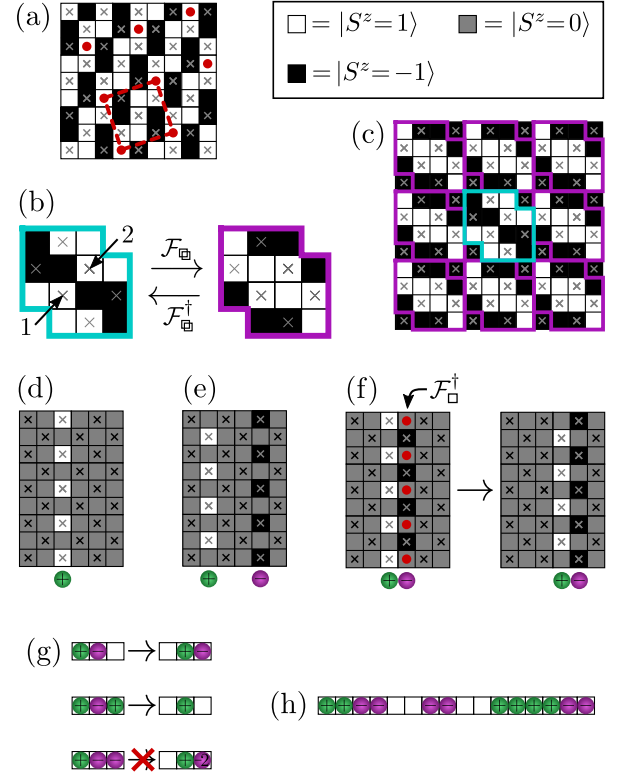


FIG. 1. (a) Spin configuration with the largest density of non-overlapping flippable eight-site clusters, to estimate a lower bound for the dimension of the constrained subspace. (b) Definition of the double fluctuator $\mathcal{F}_{\boxplus}$. Note that the two sites 1 and 2 are not flipped by $\mathcal{F}_{\boxplus}$. (c) $4 \times 4$ periodic state where the action of $\mathcal{F}_{\boxplus}^{\dagger}$ in any unit cell leads to a new Hilbert space sector. (d) Single $S^z$-string charge. (e) Single $S^z$-string dipole. (f) Elementary string-dipole move generated by applying the fluctuator $\mathcal{F}_{\square}^{\dagger}$ on the eight-site clusters around the red dots. (g) Rules for string-dipole moves. While the top and middle moves are allowed, the process at the bottom is forbidden due to the spin-1 constraint $|S_i^z| \leq 1$. (h) Example of a sequence of paired string charges for proving the existence of subextensively many Hilbert-space sectors from string states in the spin-1 system.

tem. We could generally not identify any mechanism to construct exponentially many Hilbert space sectors that have non-trivial dynamics. We therefore conclude that while spin states like in Fig. 1(c) can be used to prove the existence of exponentially many sectors, they are highly artificial and the total number of states they contain only cover a small part of the constrained Hilbert space.

On the other hand, there exists a way to construct subextensively many sectors (i.e., whose number scales exponentially with the linear system size $L$) which have non-trivial and collective dynamics, possibly hosting a fracton spin liquid. Their construction is based on the string-like configuration on sublattice 1 shown in Fig. 1(d). In the following, we define the operator $\mathcal{G}_{|} = \prod S_{\boxtimes}^{+}$, which creates such a string when acting on a homogeneous $S_i^z = 0$ state. We assign a 'string-charge' $\mathcal{Q} = \pm 1$ to these states,

indicating whether the strings are built from $S_i^z = 1$ or from $S_i^z = -1$ states. We call such configurations '$S^z$-strings' and mark them with green balls (for $\mathcal{Q} = +1$) or violet balls (for $\mathcal{Q} = -1$) in Fig. 1(d)-(h). The term 'charge' in this context should not be confused with the fractonic matter charges $\rho$. All configurations with one or more strings are translation invariant in $y$-direction and fulfill all constraints $\mathcal{C}_\boxtimes = 0$. The following discussion only considers such translation invariant states and treats them as representative states for the entire Hilbert space sectors they belong to, in which $y$-translation invariance of individual states is typically broken. In a similar way, our arguments also hold for horizontal or diagonal strings (note, however, that a diagonal string has to be defined on sublattice 2 in order to respect all ground state constraints).

The operator $\mathcal{G}_|$ does not commute with the conserved subdimensional magnetizations $M_\searrow$, $M_\nearrow$ in Fig. 2 of the main text and thus cannot be constructed by repeated applications of $\mathcal{F}_\square$. Therefore, adding a $S^z$-string generates a new Hilbert-space sector. Next, we consider a string-dipole consisting of a $\mathcal{Q} = +1$ string and a $\mathcal{Q} = -1$ string as shown in Fig. 1(e) which is created by the operator $\mathcal{G}_{|_1}\mathcal{G}_{|_2}^\dagger$. Since such operators can also not be built from individual fluctuators $\mathcal{F}_\square$, because this would require *fractional* fluctuator moves (see discussion in Fig. 2 of Ref. [1]), adding a string-dipole gives again rise to a new Hilbert space sector. The simplest change of one string configuration into another, which does *not* create a new Hilbert space sector is the translation of a string-dipole in the perpendicular direction as shown in Fig. 1(f). This string-dipole move can be generated by applying fluctuators $\mathcal{F}_\square^\dagger$ on the eight-site clusters around the red dots in Fig. 1(f) and corresponds to the insertion of a string-quadrupole.

Importantly, however, this motion of string dipoles is restricted by the spin constraint $S_i^z \in \{-1, 0, 1\}$. To see this we summarize the rules for string moves in Fig. 1(g) where we only show the effective one-dimensional system of green/violet string charges along the $x$-direction and omit the $y$-direction. The move illustrated in the top panel of Fig. 1(g) is just the elementary dipole translation of Fig. 1(f). The middle panel of Fig. 1(g) also shows an allowed elementary dipole move where the '$+-$' dipole in the sequence '$+-+$' is moved to the right by one lattice spacing involving the annihilation of a positive and negative string-charge. On the other hand, as shown in the bottom panel of Fig. 1(g), a '$+-$' dipole cannot be moved to the right when it is blocked by another '$-$' string charge, as this would generate sites with $S_i^z = -2$. Therefore, a string dipole cannot be moved across a single string-charge by fluctuator moves $\mathcal{F}_\square$.

This blocking effect in the motion of string-dipoles due to the spin length constraint gives rise to a subextensive scaling of the number of Hilbert-space sectors. To understand this and to estimate a lower bound for the number of sectors we consider a *subset* of all possible string configurations in which all arrangements of string charges
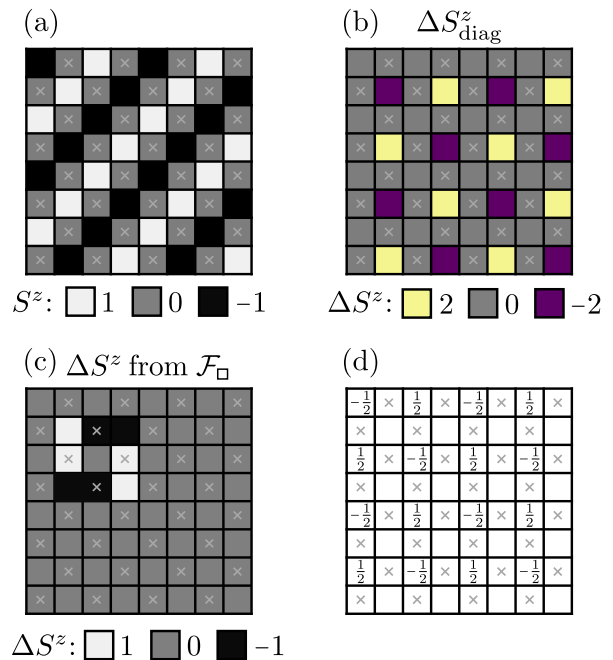


FIG. 2. (a) 90° rotated version of the diagonal stripe state in Fig. 3(a) of the main text. (b) Difference $\Delta S_{\text{diag}}^z$ between the diagonal stripe states in Fig. 3(a) of the main text and in (a). (c) Spin changes $\Delta S^z$ from the application of $\mathcal{F}_\square$ in one eight-site cluster. (d) Multiplicities of the applications of $\mathcal{F}_\square$ to generate $\Delta S_{\text{diag}}^z$ in (b).

($\mathcal{Q} = -1$, $\mathcal{Q} = 0$ or $\mathcal{Q} = +1$) occur in nearest neighbor pairs of equal charges [see Fig. 1(h) for an example]. Importantly, dipole motion is completely blocked in all of these states due to the forbidden process in the bottom panel of Fig. 1(g) such that different states cannot be transformed into each other by $\mathcal{F}_\square$ moves. Therefore, each of these paired string configurations can be regarded as a representative state in distinct Hilbert-space sectors. The number of these configurations scales subextensively as $3^{L_x/2}$ where the base 3 stands for the three possible charges $\mathcal{Q} = -1$, $\mathcal{Q} = 0$ or $\mathcal{Q} = +1$ and the factor $1/2$ in the exponent is due to the pairing of strings.

Crucially, in contrast to the extensively many sectors constructed via the double moves $\mathcal{F}_\boxplus$, the subextensively many sectors from string configurations usually allow for non-trivial, collective dynamics with overlapping fluctuator moves $\mathcal{F}_\square$. We expect that all states in the subextensively many string sectors altogether cover a much larger part of the constrained Hilbert space than the sectors from $\mathcal{F}_\boxplus$-moves.

## III. DYNAMICALLY DISCONNECTED DIAGONAL STRIPE SECTORS

Here we show that 90° rotated versions of the diagonal stripe state lie in dynamically disconnected sectors under the action of $\mathcal{F}_\square$ and $\mathcal{F}_\square^\dagger$. This property explains

the broken 90° rotation symmetry of the spin structure factor in Fig. 5(a) of the main text and shows that this asymmetry is not a consequence of spontaneous lattice symmetry breaking, but rather due to the asymmetry of the diagonal stripe state itself.

In Fig. 2(a) we show a 90° rotated version of the diagonal stripe state in Fig. 3(a) of the main text. For the system to tunnel between both states, the $z$-components of the spins have to change by the amount illustrated in Fig. 2(b), where $\Delta S^z_{\text{diag}}$ is the difference between the diagonal stripe state in Fig. 3(a) of the main text and the one in Fig. 2(a). In a tunneling process this difference has to be generated by repeated actions of $\mathcal{F}_\square$ (or $\mathcal{F}_\square^\dagger$) on the different eight-site clusters $\square$. As an example, the change $\Delta S^z$ from $\mathcal{F}_\square$ for one particular eight-site cluster $\square$ is illustrated in Fig. 2(c). The problem of describing this tunneling process with $\mathcal{F}_\square$ can be considered as a linear algebra problem that consists of finding a linear combination of the eight-site changes $\Delta S^z$ in Fig. 2(c) that yields $\Delta S^z_{\text{diag}}$ in Fig. 2(b). It needs to be taken into account that the $N_{\text{sites}}/2$ fluctuators $\mathcal{F}_\square$ on all clusters $\square$ are not linearly independent but have rank $N_{\text{sites}}/2 - 1$, as discussed in detail in Sec. II.B in Ref. [1]. Therefore, to find a unique solution, one of the fluctuators $\mathcal{F}_\square$ needs to be omitted to ensure that the other fluctuators $\mathcal{F}_\square$ form a set of basis vectors for the local moves in the constrained subspace. Here, without loss of generality, we have omitted the fluctuator in row 1, column 2 (when counted from the bottom left corner) of the lattice array in Fig. 2. The solution to express $\Delta S^z_{\text{diag}}$ via local fluctuators, obtained by simple matrix inversion, is illustrated in Fig. 2(d) where the numbers $a$ on the sublattice 2 sites $\square$ correspond to the multiplicities $(\mathcal{F}_\square)^a$ with which the integer spin changes $\Delta S^z$ in the eight-site clusters have to be applied. Importantly, these multiplicities contain *non-integer* $a = \pm 1/2$ values, showing that fractional applications of $\mathcal{F}_\square$ would be needed to tunnel between both states. In other words, no sequential applications of $\mathcal{F}_\square$ exist that can realize this process and, consequently, both diagonal stripe states lie in different Hilbert space sectors. This result is independent of the choice of fluctuator $\mathcal{F}_\square$ that is omitted in the set of basis vectors.

We note that in addition to 90° rotated versions of diagonal stripe states, also time-reversed ($S^z \rightarrow -S^z$) versions exist. However, time-reversed partners of diagonal stripe states are found to be in the *same* Hilbert space sector, which implies that the diagonal stripe order at $\mu < 0.8J'$ in Fig. 4 of the main text is associated with spontaneous time-reversal symmetry breaking.

## IV. MAXIMALLY FLIPPABLE STATES IN THE $6 \times 6$ SECTOR

The observation of broken ergodicity at low $\mu$ in the sector of the $6 \times 6$ state in Fig. 3(c) of the main text is related to the system's inability to exhibit $4 \times 4$ order: While the $6 \times 6$ state has a large number of flippable
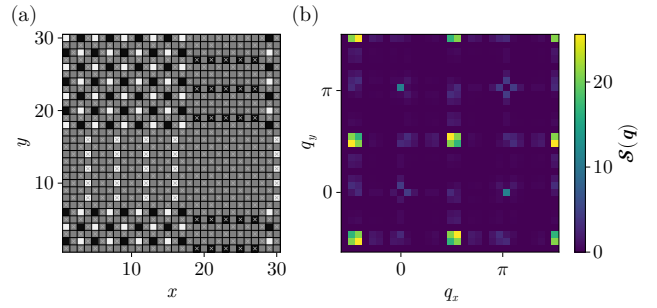


FIG. 3. (a) One of the maximally flippable states found in the $6 \times 6$ sector and (b) its corresponding spin structure factor $\mathcal{S}(\boldsymbol{q})$.

clusters, numerical results indicate that other, more complicated, configurations exist in this sector with an even larger number. These configurations, such as the one shown in Fig. 3(a), and configurations related by lattice symmetries, are separated by large energetic barriers for small $\mu$, leading to exceedingly large autocorrelation times. At larger values $\mu$, energetic barriers are lowered, while fluctuations between larger networks of spin configuration are favorable, allowing for ergodic quantum tunneling within the entire sector. In order to find this configuration, we initialized 3840 independent GFMC simulations at $\mu = 0$ with a single walker and recorded each configuration encountered. To confirm that the correct solution was found, we repeated this procedure five times, finding equivalent configurations (up to lattice translations). The result is shown in Fig. 3(a), featuring a phase separation effect with a large domain with a $4 \times 4$ order. By computing $\mathcal{S}(\boldsymbol{q})$ for this configuration [Fig. 3(b)], we may explain the features at $\boldsymbol{q} = (\pi/L, \pi/L)$ and symmetry-related points in Fig. 6(a) of the main text, as a result of the large size of the magnetic domains. On the other hand, this configuration still shows a strong peak at $\boldsymbol{q} = (\pi, \pi)$ which is however difficult to resolve in Fig. 6(a) of the main text due to the considerable uncertainties resulting from the broken ergodicity.

## V. DETAILS ON THE EFFECTIVE RANK-2 U(1) FIELD THEORY

Our Maxwellian field theory in Eq. (9) of the main text is derived by expressing the spin flip operators in $\mathcal{H}_2$ in terms of rotor variables $S_i^\pm = \sqrt{2}e^{\pm \imath A_i^{\hat{\alpha}}}$ where $A_i^\alpha$ takes the role of a generalized 'vector' potential. The operators $A_i^\alpha$ (which follow the convention that $\alpha = xy$ when $i$ is on sublattice 1 and $\alpha = xx$ when $i$ is on sublattice 2) are the components of a trace-free and symmetric matrix-valued field, i.e., $A_i^{xx} = -A_i^{yy}$ and $A_i^{xy} = A_i^{yx}$. Furthermore, $A_i^\alpha$ is compact, i.e., its eigenvalues lie in the interval $[0, 2\pi]$. The $z$-components of the spins $S_i^z$ take the role of a con-

jugate integer-valued matrix electric field $S_i^z = E_i^\alpha$ with $[A_i^\alpha, E_i^\alpha] = \imath$. Note that when $i$ is on sublattice 1 (2), we also use the notation $A_i^{xy} \equiv A_\boxtimes^{xy}$ ($A_i^{xx} \equiv A_\square^{xx}$) and equivalently for $E_i^\alpha$. With these definitions $\mathcal{H}_2$ has the form

$$\mathcal{H}_2 \sim -\sum_\square \cos B_\square \sim +\sum_\square B_\square^2 \qquad (3)$$

where $B_\square$ is defined for each cluster $\square$ as given in Eq. (8) of the main text and the rightmost expression in Eq. (18) of the main text represents the expansion of $\mathcal{H}_2$ in lowest non-trivial order in $B_\square$. Furthermore, in order to suppress electric field states $E_i^\alpha \notin \{-1, 0, 1\}$, a term $\sim \sum_i (E_i^\alpha)^2$ in the field theory is required. Together with the RK potential $\sim \sum_\square \mathcal{N}_\square^2$ this yields the effective field theory in Eq. (9) of the main text. An important property of this theory that distinguishes it from conventional U(1) gauge theories is the absence of electromagnetic duality. This is already evident from the different properties of the electric and magnetic fields where the former is a matrix while the latter is a one-component object.

Note that our mapping to an effective field theory could, in principle, also be applied to the spin-1/2 spiderweb model. This would require a change of the (irrelevant) prefactor $\sqrt{2}$ in Eq. (6) of the main text and a redefinition of the electric field to ensure that it only assumes integer values. The resulting field theory, known e.g. from spin-1/2 quantum spin ice, is called 'frustrated' [9] due to the lack of a well-defined vacuum of electric fields. On the other hand, our field theory for a spin-1 system has the advantage of a unique vacuum state corresponding to the homogeneous $S_i^z = 0$ configuration.

The field theory has a local gauge freedom that follows from the rank-2 Gauss' law and amounts to the invariance under the operation [10]

$$U(f_\boxtimes) = \exp\left(\imath \sum_\boxtimes f_\boxtimes \mathcal{C}_\boxtimes\right) \qquad (4)$$

where $f_\boxtimes$ is an arbitrary function defined for each cluster $\boxtimes$ or, stated differently, $f_\boxtimes$ is located on sublattice 1. To see this, we use

$$\mathcal{C}_\boxtimes = E_{\boxtimes_1}^{xx} + E_{\boxtimes_2}^{xy} - E_{\boxtimes_3}^{xx} - E_{\boxtimes_4}^{xy} + E_{\boxtimes_5}^{xx} + E_{\boxtimes_6}^{xy} - E_{\boxtimes_7}^{xx} - E_{\boxtimes_8}^{xy} \quad (5)$$

and rearrange the sum in the exponent of Eq. (4), yielding

$$U(f_\boxtimes) = \exp\left[\imath \sum_\boxtimes E_\boxtimes^{xy}(f_{\boxtimes_2} - f_{\boxtimes_4} + f_{\boxtimes_6} - f_{\boxtimes_8})\right] \times$$
$$\exp\left[\imath \sum_\square E_\square^{xx}(f_{\square_1} - f_{\square_3} + f_{\square_5} - f_{\square_7})\right]. \quad (6)$$

Here, the labels $\boxtimes_a$ and $\square_a$ use the convention explained below Eq. (2) of the main text where, e.g., $f_{\square_1}$ is a site to the right of the center of a $\square$ cluster, such that $f_{\square_1}$ is still defined on sublattice 1 (center of a $\boxtimes$ cluster). Since

| Quantities on sublattice 1 | Quantities on sublattice 2 |
|---|---|
| (= center of $\boxtimes$ clusters): | (= center of $\square$ clusters): |
| $\mathcal{C}$ (constraint) | $\mathcal{F}$ (fluctuator) |
| $\rho$ (fractons) | $B$ (magnetic field) |
| $A^{xy}$, $E^{xy}$ | $A^{xx}$, $E^{xx}$ |
| (fields of U(1) theory) | (fields of U(1) theory) |
| $f$ (gauge transformation) | $\mathcal{N}^2$ (RK potential) |

TABLE II. Definitions of the two sublattices of the spiderweb model and location of different quantities.

$\exp(\imath\theta E_i^\alpha)$ with $\theta \in \mathbb{R}$ shifts $A_i^\alpha \to A_i^\alpha + \theta$, the operation in Eq. (6) can be written as

$$A_\boxtimes^{xy} \to A_\boxtimes^{xy} + f_{\boxtimes_2} - f_{\boxtimes_4} + f_{\boxtimes_6} - f_{\boxtimes_8},$$
$$A_\square^{xx} \to A_\square^{xx} + f_{\square_1} - f_{\square_3} + f_{\square_5} - f_{\square_7}. \quad (7)$$

By simple bookkeeping of all terms it can be checked that Eq. (8) of the main text is indeed invariant under this transformation.

In Table II we list all the quantities occurring in the spiderweb model and in the effective field theory and we specify the sublattice on which they are defined.

The gauge transformation in Eq. (7) becomes more transparent in a continuum description where it reads

$$A^{xy} \to A^{xy} + 4\partial_x\partial_y f,$$
$$A^{xx} \to A^{xx} + (\partial_x^2 - \partial_y^2)f. \quad (8)$$

Using the continuum definition of the magnetic field in Eq. (8) of the main text,

$$B = -4\partial_x\partial_y A^{xx} + (\partial_x^2 - \partial_y^2)A^{xy}, \quad (9)$$

the invariance of $B$ under the gauge transformation in Eq. (8) is immediately obvious. The special property of Eq. (9) is that $B$ is constructed from *second* derivatives of $A^{xx}$ and $A^{xy}$. This is in contrast to a three-dimensional scalar charge rank-1 or rank-2 U(1) gauge theory where one derivative is sufficient to construct a gauge invariant magnetic field [11]. The relation between $B$ and $A^{\mu\nu}$ in Eq. (9) also makes the lack of Lorentz-invariance of the effective field theory apparent. To see this, we consider the system's Lagrangian $\mathcal{L}$ which contains a term $\sim (\partial_t A^{\mu\nu})^2$ with a first derivative in time describing the electric field contribution $(E^{\mu\nu})^2$. Furthermore, $\mathcal{L}$ contains a term $\sim B^2$ which, according to Eq. (9), contains second spatial derivatives. This unequal treatment of space and time is incompatible with Lorentz invariance.

Returning to the lattice version of our rank-2 U(1) gauge theory [see Eq. (9) of the main text], this Hamiltonian describes a Gaussian theory whose eigenmodes can be calculated analytically. To this end we rewrite $A_i^\alpha$ and $E_i^\alpha$ in terms of bosonic operators $a_i^\alpha$, $(a_i^\alpha)^\dagger$,

$$A_i^\alpha = \frac{1}{\sqrt{2}}\left[a_i^\alpha + (a_i^\alpha)^\dagger\right], \quad E_i^\alpha = \frac{1}{\sqrt{2}\imath}\left[a_i^\alpha - (a_i^\alpha)^\dagger\right], \quad (10)$$

which fulfill the standard commutation relation $[a_i^\alpha, (a_i^\alpha)^\dagger] = 1$. Furthermore, we Fourier-transform the bosonic operators using

$$a_i^\alpha = \sqrt{\frac{2}{N_{\text{sites}}}} \sum_{\boldsymbol{q}} e^{\imath \boldsymbol{q} \cdot \boldsymbol{r}_i} a^\alpha(\boldsymbol{q}) . \quad (11)$$

Here, $\boldsymbol{r}_i$ is the real-space position of site $i$ and the sum only includes momenta $\boldsymbol{q}$ in the first Brillouin zone. Note that our model consists of two inequivalent sublattices such that the first Brillouin zone can, for example, be chosen as $q_x \in [-\pi/2, \pi/2]$, $q_y \in [-\pi, \pi]$. With these definitions, $\mathcal{H}_{\text{eff}}$ from Eq. (9) of the main text can be written as

$$\mathcal{H}_{\text{eff}} = \sum_{\boldsymbol{q}} A^\dagger(\boldsymbol{q}) H_{\text{eff}} A(\boldsymbol{q}) , \quad (12)$$

where $A(\boldsymbol{q})$ is a four-component operator

$$A(\boldsymbol{q}) = (a^{xy}(\boldsymbol{q}), a^{xx}(\boldsymbol{q}), [a^{xy}(-\boldsymbol{q})]^\dagger, [a^{xx}(-\boldsymbol{q})]^\dagger) \quad (13)$$

and the $4 \times 4$ matrix $H_{\text{eff}}$ is given by

$$H_{\text{eff}} = K V_+^T V_+ + W V_-^T V_- + \frac{U}{4} \begin{pmatrix} 1 & 0 & -1 & 0 \\ 0 & 1 & 0 & -1 \\ -1 & 0 & 1 & 0 \\ 0 & -1 & 0 & 1 \end{pmatrix} \quad (14)$$

with

$$V_\pm = (c_x - c_y, 2s_x s_y, \pm(c_x - c_y), \pm 2s_x s_y) \quad (15)$$

and $c_\mu = \cos q_\mu$, $s_\mu = \sin q_\mu$ with $\mu = x, y$.

According to the standard procedure of a Bogoliubov transformation, to solve the model, we need to rewrite $\mathcal{H}_{\text{eff}}$ in terms of Bose operators $C(\boldsymbol{q})$ for the eigenmodes,

$$C(\boldsymbol{q}) = (c_1(\boldsymbol{q}), c_2(\boldsymbol{q}), c_1^\dagger(\boldsymbol{q}), c_2^\dagger(\boldsymbol{q})) \quad (16)$$

where $C(\boldsymbol{q}) = \mathcal{J}(\boldsymbol{q}) A(\boldsymbol{q})$ such that $(\mathcal{J}^\dagger)^{-1} H_{\text{eff}} \mathcal{J}^{-1}$ is diagonal. Note that, to preserve the bosonic commutation relations of $C(\boldsymbol{q})$, the $4 \times 4$ matrix $\mathcal{J}(\boldsymbol{q})$ needs to be a *paraunitary* transformation that satisfies $\mathcal{J}^\dagger g \mathcal{J} = g$ with $g = \text{diag}(1, 1, -1, -1)$ [12]. A subtlety arises because of the gauge invariance of $\mathcal{H}_{\text{eff}}$ which manifests in a bosonic zero mode. Since a paraunitary transformation $\mathcal{J}(\boldsymbol{q})$ is not defined in this case, we introduce an additional term in the Hamiltonian of the form $2d \sum_i (A_i^\alpha)^2$ which breaks gauge invariance and which allows us to explicitly calculate $\mathcal{J}(\boldsymbol{q})$. The gauge-invariant limit $d \to 0$ can be recovered at the end of the calculation. The transformation matrix $\mathcal{J}(\boldsymbol{q})$ is found to be

$$\mathcal{J}(\boldsymbol{q}) = \frac{1}{\sqrt{8(L_1^2 + L_2^2)}} \times$$

$$\times \begin{pmatrix} L_1 \xi_+ & L_2 \xi_+ & -L_1 \xi_- & -L_2 \xi_- \\ -L_2 \lambda_+ & L_1 \lambda_+ & L_2 \lambda_- & -L_1 \lambda_- \\ -L_1 \xi_- & -L_2 \xi_- & L_1 \xi_+ & L_2 \xi_+ \\ L_2 \lambda_- & -L_1 \lambda_- & -L_2 \lambda_+ & L_1 \lambda_+ \end{pmatrix} \quad (17)$$

with

$$\xi_\pm = \left(\frac{U}{d}\right)^{1/4} \pm 2\left(\frac{d}{U}\right)^{1/4} , \quad (18)$$

$$\lambda_\pm = \sqrt{2}\left[\left(\frac{\eta_2}{\eta_1}\right)^{1/4} \pm \left(\frac{\eta_1}{\eta_2}\right)^{1/4}\right] , \quad (19)$$

$$\eta_1 = d + K\left[(c_x - c_y)^2 + 4s_x^2 s_y^2\right] , \quad (20)$$

$$\eta_2 = \frac{U}{4} + W\left[(c_x - c_y)^2 + 4s_x^2 s_y^2\right] , \quad (21)$$

and $L_1$, $L_2$ are the components of the *constraint vector* [1], given by

$$\begin{aligned} L_1(\boldsymbol{q}) &= -4\sin q_x \sin q_y , \\ L_2(\boldsymbol{q}) &= 2(\cos q_x - \cos q_y) . \end{aligned} \quad (22)$$

Diagonalizing $H_{\text{eff}}$ with $\mathcal{J}$ leads in the limit $d \to 0$ to a zero mode due to the system's gauge freedom and a single photon mode with the dispersion

$$\begin{aligned} \omega(\boldsymbol{q}) &= 2\sqrt{\eta_1 \eta_2} \\ &= 2\sqrt{K\left[(c_x - c_y)^2 + 4s_x^2 s_y^2\right]} \times \\ &\quad \times \sqrt{\frac{U}{4} + W\left[(c_x - c_y)^2 + 4s_x^2 s_y^2\right]}. \end{aligned} \quad (23)$$

This photon dispersion is gapless at $\boldsymbol{q} = (0,0)$ and $\boldsymbol{q} = (\pi,\pi)$. An expansion of $\omega(\boldsymbol{q})$ around these two points yields for $U \neq 0$ in lowest non-vanishing order

$$\omega(\boldsymbol{q}) \approx \sqrt{\frac{KU}{4}} \sqrt{q_x^4 + 14q_x^2 q_y^2 + q_y^4} . \quad (24)$$

This function is quadratic in any radial direction away from the gapless points, however, it does not have a continuous rotation symmetry around these points, as discussed in Sec. II.A in Ref. [1]. On the other hand, exactly at the RK-point $U = 0$, the photon dispersion becomes quartic at long wavelengths,

$$\omega(\boldsymbol{q}) \approx \sqrt{\frac{KW}{4}} \left(q_x^4 + 14q_x^2 q_y^2 + q_y^4\right) . \quad (25)$$

Another prediction of the field theory is the spin structure factor

$$S(\boldsymbol{q}) = \frac{1}{N_{\text{sites}}} \sum_{i,j} \langle S_i^z S_j^z \rangle e^{\imath \boldsymbol{q} \cdot (\boldsymbol{r}_i - \boldsymbol{r}_j)}, \quad (26)$$

which can be obtained by expressing the spin operators $S_i^z$ in terms of $a_i^\alpha$, $(a_i^\alpha)^\dagger$ bosons [Eq. (7) of the main text and Eq. (10)], transforming them into the eigenbasis of $C$ bosons using the matrix $\mathcal{J}$ and exploiting that the groundstate is free of any photon excitations. For $d \to 0$ this yields

$$\begin{aligned} S(\boldsymbol{q}) &= \sqrt{\frac{\eta_1}{\eta_2}} \frac{(L_1 - L_2)^2}{L_1^2 + L_2^2} \\ &= \frac{\sqrt{K}(c_x - c_y + 2s_x s_y)^2}{\sqrt{(c_x - c_y)^2 + 4s_x^2 s_y^2}\sqrt{\frac{U}{4} + W\left[(c_x - c_y)^2 + 4s_x^2 s_y^2\right]}}. \end{aligned} \quad (27)$$

Note that for fitting this function to numerical results, we need to define only two truly independent fitting parameters $(A, r)$ via $(K, W, U) = (4A^2, 1, r)$, where $A$ only modifies the structure factor by a global scaling, which cannot be fixed by sum rules for spin 1, and $r$ tunes the relative strength of the RK potential. In the RK limit $U \to 0$ where $\eta_1/\eta_2 = K/W$ is a constant, this expression becomes (up to a prefactor) identical to the classical spin structure factor in Gaussian approximation given by $\mathcal{S}_{\text{class}}(\boldsymbol{q}) = \frac{(c_x - c_y + 2s_x s_y)^2}{(c_x - c_y)^2 + 4s_x^2 s_y^2}$ [1]. This is expected because at the RK point a ground state can be constructed by an equal weight superposition of all $S_i^z$ basis states in a given Hilbert space sector, similar to a classical (non-coherent) superposition. Furthermore, at $W = 0$ when $\eta_2 = U/4$ is a constant, the spin structure factor in Eq. (27) corresponds to the classical result, multiplied by the photon dispersion $\omega(\boldsymbol{q})$ which suppresses the fourfold pinch points around their center. The interpolation between both limits is determined by the term

$\sqrt{U/4 + W\left[(c_x - c_y)^2 + 4s_x^2 s_y^2\right]}$ in the denominator of Eq. (27). For finite $W > 0$ there is a threshold momentum $q_c$ (which decreases with increasing $W$) above which the $W$-term dominates and the spin structure factor resembles the classical one. On the other hand, for $q \lesssim q_c$ the $U$-term dominates and the spin structure factor is suppressed.

The photon dispersion $\omega(\boldsymbol{q})$ and the spin structure factor $\mathcal{S}(\boldsymbol{q})$ of the 90° rotation symmetry broken field theory with the additional term in Eq. (12) of the main text follow straightforwardly from Eq. (23) and Eq. (27) by the replacement

$$U \to U[1 + 2p(1 + \cos(q_x - q_y))], \qquad (28)$$

where $p = U'/U$. As pointed out in the main text, we define the independent parameters $(A, r, p)$ by the relation $(K, W, U, U') = (4A^2, 1, r, pr)$, for fitting the spin structure factor of the asymmetric field theory.

[1] N. Niggemann, M. Adhikary, Y. Schaden-Thillmann, and J. Reuther, Classical fracton spin liquid and Hilbert space fragmentation in a 2D spin-1/2 model (2025), arXiv:2508.06606 [cond-mat].

[2] P. Sala, T. Rakovszky, R. Verresen, M. Knap, and F. Pollmann, Ergodicity Breaking Arising from Hilbert Space Fragmentation in Dipole-Conserving Hamiltonians, Phys. Rev. X **10**, 011047 (2020).

[3] A. Khudorozhkov, A. Tiwari, C. Chamon, and T. Neupert, Hilbert Space Fragmentation in a 2D Quantum Spin System with Subsystem Symmetries, SciPost Physics **13**, 098 (2022).

[4] C. Stahl, O. Hart, A. Khudorozhkov, and R. Nandkishore, Strong Hilbert Space Fragmentation and Fractons from Subsystem and Higher-Form Symmetries (2025), arXiv:2505.15889 [cond-mat].

[5] D. Adler, D. Wei, M. Will, K. Srakaew, S. Agrawal, P. Weckesser, R. Moessner, F. Pollmann, I. Bloch, and J. Zeiher, Observation of Hilbert space fragmentation and fractonic excitations in 2D, Nature **636**, 80 (2024).

[6] M. Will, R. Moessner, and F. Pollmann, Realization of Hilbert Space Fragmentation and Fracton Dynamics in Two Dimensions, Phys. Rev. Lett. **133**, 196301 (2024).

[7] X. Feng and B. Skinner, Hilbert space fragmentation produces an effective attraction between fractons, Phys. Rev. Res. **4**, 013053 (2022).

[8] K. Lee, A. Pal, and H. J. Changlani, Frustration-induced emergent Hilbert space fragmentation, Physical Review B **103**, 235133 (2021).

[9] M. Hermele, M. P. A. Fisher, and L. Balents, Pyrochlore photons: The $U(1)$ spin liquid in a $S = \frac{1}{2}$ three-dimensional frustrated magnet, Phys. Rev. B **69**, 064404 (2004).

[10] L. Savary and L. Balents, Quantum spin liquids: a review, Rep. Prog. Phys. **80**, 016502 (2016).

[11] M. Pretko, Generalized electromagnetism of subdimensional particles: A spin liquid story, Phys. Rev. B **96**, 035119 (2017).

[12] J. Colpa, Diagonalization of the quadratic boson hamiltonian, Physica A: Statistical Mechanics and its Applications **93**, 327 (1978).